J. Fluid Mech. (1985), *vol.* 159, *pp.* 151–168
Printed in Great Britain

Absolute and convective instabilities in free shear layers

By P. HUERRE

Department of Aerospace Engineering, University of Southern California, Los Angeles, California 90089–0192

AND P. A. MONKEWITZ

Department of Mechanical, Aerospace and Nuclear Engineering, University of California at Los Angeles, Los Angeles, California 90024

(Received 13 September 1982 and in revised form 17 April 1985)

The absolute or convective character of inviscid instabilities in parallel shear flows can be determined by examining the branch-point singularities of the dispersion relation for complex frequencies and wavenumbers. According to a criterion developed in the study of plasma instabilities, a flow is convectively unstable when the branch-point singularities are in the lower half complex-frequency plane. These concepts are applied to a family of free shear layers with varying velocity ratio $R = \Delta U/2\overline{U}$, where ΔU is the velocity difference between the two streams and $\overline{U}$ their average velocity. It is demonstrated that spatially growing waves can only be observed if the mixing layer is convectively unstable, i.e. when the velocity ratio is smaller than $R_t = 1.315$. When the velocity ratio is larger than R_t, the instability develops temporally. Finally, the implications of these concepts are discussed also for wakes and hot jets.

1. Introduction

Linear stability theory has been extremely successful in predicting many essential features of the initial development of a variety of flow instabilities. In any such comparison one has to choose between temporal theory and spatial theory. In temporal stability calculations it is implicitly assumed that disturbances evolve in time from some initial spatial distribution. The wavenumber k is taken to be real and the goal of linear theory is then to determine the complex frequency ω as a function of k. This point of view is usually adopted in theoretical investigations of Taylor–Couette flow and Rayleigh–Bénard convection. However, in the study of parallel-flow instabilities such as free shear flows and boundary layers, the instability process is very often controlled by periodically forcing the flow at a given frequency. Experimental results then seem to follow much more closely the predictions of spatial theory, where the frequency ω is real and the wavenumber k is complex.

The basic purpose of the present investigation is to describe a methodology that, for any flow configuration, determines whether spatial stability theory is applicable. The study is presented in the particular framework of the linear instability of inviscid parallel shear flows. The application of the results to a one-parameter family of mixing layers clearly demonstrates that one cannot rely merely on physical intuition to decide if spatial waves are relevant.

We shall follow the terminology introduced by Briggs (1964) and Bers (1975) in

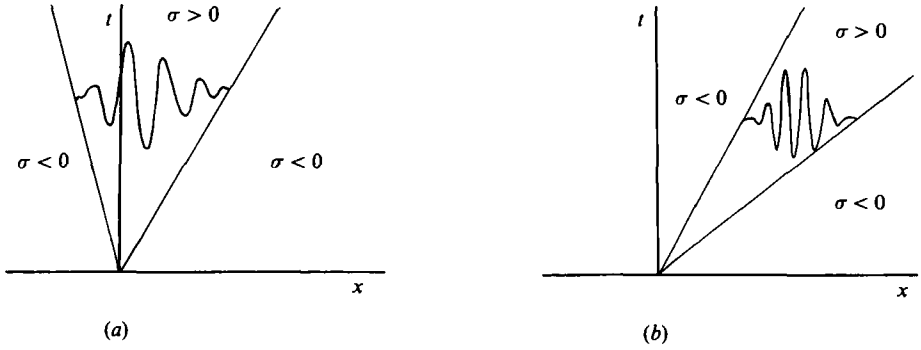

FIGURE 1. Sketch of a typical impulse response: (*a*) absolutely unstable flow; (*b*) convectively unstable flow.

the study of plasma instabilities and distinguish between absolutely unstable media and convectively unstable media (see also Drazin & Reid 1981, §24). The impulse response, or Green function g (see §2), of a flow is first defined as the instability-wave field generated by a Dirac delta function in space and time. A flow is then absolutely unstable if its impulse response (figure 1*a*) becomes unbounded for large time at all points. A flow is convectively unstable if its impulse response (figure 1*b*) decays to zero for large time at all points in the flow. In other words, in absolutely unstable flows the presence of a transient disturbance at any location leads, in the linear regime, to exponential growth everywhere. By contrast, in convectively unstable flows disturbances are convected away as they amplify, eventually leaving the basic flow undisturbed. We note that, in agreement with these definitions, experimenters take extreme care in introducing a probe in any absolutely unstable system such as Taylor–Couette flow or Bénard convection. Any small disturbance could dramatically alter the nature of the flow.

A clarification of the role of spatially growing modes can then be obtained from a study of the signalling problem (§3), where instability waves are periodically forced at a specific location. In the absolutely unstable case any transients generated by switching on the excitation or any residual background fluctuations will amplify and contaminate the entire flow, thereby leading to a zero signal-to-noise ratio. In the convectively unstable case, however, these transients and background fluctuations are convected downstream, and spatially growing waves at the excitation frequency can be observed. Hence spatially growing waves are only meaningful physically in convectively unstable flows. It can also be concluded that a choice between spatial and temporal (or more precisely *non*-spatial) theory can be made once the absolute or convective nature of the instability has been determined.

According to the criterion (§2) derived in a general context by Bers (1975), a flow is convectively unstable if the modes of complex frequency and wavenumber, which have a zero group velocity, are all temporally damped, i.e. the corresponding complex frequencies are all in the lower half ω-plane. A satisfactory answer to the present problem therefore requires not only knowledge of the properties of temporal and spatial waves, but also knowledge of the singularities of the dispersion relation for complex frequencies and wavenumbers.

The asymptotic behaviour of the impulse response in boundary layers, as calculated by Gaster (1968, 1975, 1980), has provided an accurate description of the evolution

of wave packets in the linear regime. We must point out, however, that the concepts of absolute and convective instability have not been extensively used in hydrodynamic-stability investigations (for an application to a geophysical flow, see Merkine 1977). It is felt that they allow a rigorous justification of the use of spatially growing waves, as discussed in more detail in §3, and lead to a convenient and physically meaningful (§5) classification of possible linear instabilities.

2. A criterion for convective or absolute instability

In this section the calculation of the asymptotic impulse response is first outlined. A criterion is then developed that unambiguously determines whether a given velocity profile is convectively or absolutely unstable.

The approach follows the formulation of the initial-value problem adopted by Case (1960) and Drazin & Howard (1966) for a homogeneous fluid. The case of a stratified fluid has recently been examined by Chimonas (1979) and Brown & Stewartson (1980). The instability is assumed to be inviscid and governed by the usual linearized two-dimensional vorticity equation, written in terms of a perturbation stream function. The variables x and y denote the streamwise and cross-stream directions respectively and t is the time variable. By definition the impulse response or real Green function $g(x, y, t; y_0)$ pertaining to the velocity profile $U(y)$ satisfies the forced equation

$$\mathscr{L}[g] \equiv \left[\frac{\partial}{\partial t} + U(y)\frac{\partial}{\partial x}\right]\nabla^2 g - U''(y)\frac{\partial g}{\partial x} = \delta(x)\,\delta(y-y_0)\,\delta(t), \tag{1}$$

which, for unbounded mixing layers, must be supplemented by requiring exponential decay of g as $y \to \pm\infty$. The Dirac delta functions represent a point source at $x = 0$, $y = y_0$ and the response is required to be causal, i.e. $g = 0$ when $t < 0$. If g is known, the response of the flow to an arbitrary source distribution $s(x, y, t)$ can be obtained by convolution of s and g.

With the real function $g(x, y, t; y_0)$, we associate the complex Green function $G(x, y, t; y_0)$ with g as real part and the Hilbert transform of g as imaginary part. Using the notation $f * g$ for the spatial convolution

$$\int_{-\infty}^{\infty} f(x-\xi)\,h(\xi)\,d\xi,$$

G is defined by

$$G = \left(1 + \frac{\mathrm{i}}{\pi x} *\right) g. \tag{2}$$

The complex Green function G essentially generalizes to an arbitrary wavenumber distribution, the complex representation commonly adopted for distributions containing a single wavenumber: its Fourier transform in wavenumber space is zero for negative wavenumbers. Furthermore, the physically meaningful real Green function g is obtained from G as

$$g = \mathrm{Re}\, G. \tag{3}$$

For convenience all calculations will be performed on G, which can easily be seen to satisfy

$$\mathscr{L}[G] = \left[\delta(x) + \frac{\mathrm{i}}{\pi x}\right]\delta(y-y_0)\,\delta(t). \tag{4}$$

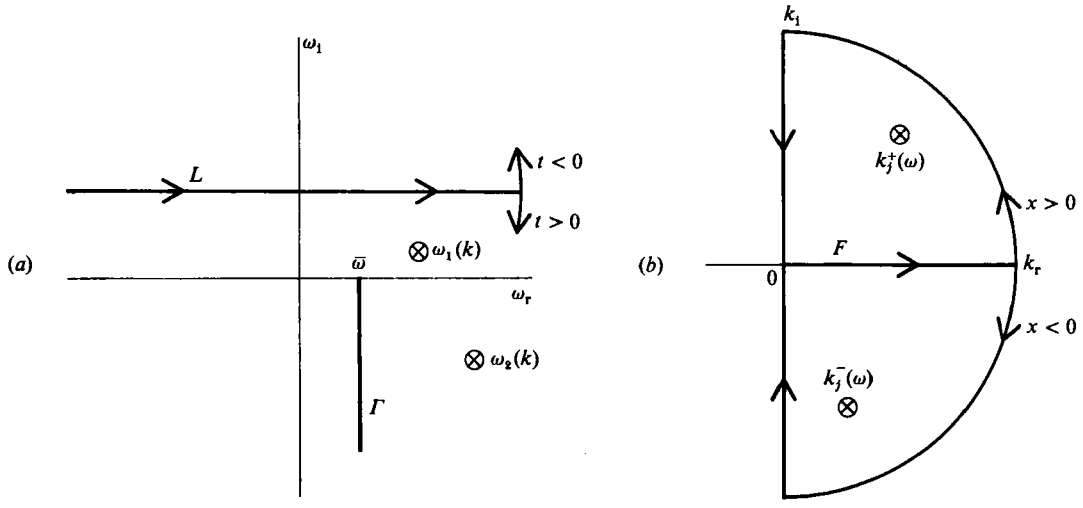

FIGURE 2. Paths of integration of the inverse Fourier transforms (5) and (6): (*a*) complex-frequency plane; (*b*) complex-wavenumber plane.

Fourier-transform pairs in space x and time t are then introduced, according to the definitions

$$G(x, y, t; y_0) = \frac{1}{2\pi}\int_F \hat{G}(k, y, t; y_0)\, e^{ikx}\, dk, \tag{5}$$

and

$$\hat{G}(k, y, t; y_0) = \frac{1}{2\pi}\int_L \hat{\hat{G}}(k, y, \omega; y_0)\, e^{-i\omega t}\, d\omega. \tag{6}$$

In (5), $\hat{G} = 0$ when $k < 0$, and the path F in the plane of complex wavenumbers k is initially taken to be the *positive* real-k axis. In order to apply the method of steepest descent, it will be closed at infinity by a quarter-circle in the upper half k-plane ($x > 0$) or lower half k-plane ($x < 0$), as shown in figure 2(*b*). The contour L in the plane of complex frequencies ω is chosen to be a straight line lying above all the singularities, so as to satisfy causality. When $t > 0$ it is closed by a semicircle below L, as indicated in figure 2(*a*).

Application of the transforms (5) and (6) to (4) leads to the forced Rayleigh equation

$$\mathrm{L}[\hat{\hat{G}}] \equiv \left[\frac{\partial^2}{\partial y^2} - k^2 - \frac{U''(y)}{U(y)-c}\right]\hat{\hat{G}}(k, y, \omega; y_0) = \frac{2H(k)\,\delta(y-y_0)}{ik[U(y_0)-c]}, \tag{7}$$

with $\hat{\hat{G}}$ being exponentially small at $y = \pm\infty$. The quantity $c = \omega/k$ is termed the complex phase velocity or phase velocity in short and $H(k)$ denotes the Heaviside unit step function. The solution of (7) is, within a constant of proportionality, the Green function of the Rayleigh equation

$$\hat{\hat{G}}(k, y, \omega; y_0) = \frac{-2H(k)}{ik[U(y_0)-c]\,D(\omega, k; y_0)} \begin{cases} \Phi_+(k, y, \omega)\,\Phi_-(k, y_0, \omega) & (y > y_0), \\ \Phi_+(k, y_0, \omega)\,\Phi_-(k, y, \omega) & (y < y_0), \end{cases} \tag{8}$$

where Φ_+ and Φ_- are solutions of the Rayleigh equation which decay exponentially as $y \to +\infty$ and $y \to -\infty$ respectively. The Wronskian $D(\omega, k; y_0)$ of Φ_+ and Φ_-, when set equal to zero, is nothing but the complex dispersion relation satisfied by the

discrete eigenvalues of the Rayleigh equation. At this point it also becomes clear why, in the above derivations, the wavenumber k has to be restricted explicitly to values with *positive real part* which, again, is always possible for real signals. The reason is that, for unbounded flows, $\hat{G}$ is in general non-analytic in k on the imaginary axis $k_r = 0$. This non-analyticity stems from the boundary condition far away from the centre of the shear layer where $\Phi_\pm \sim \exp[\mp \operatorname{sgn}(k_r)\, ky]$ as $y \to \pm\infty$.

The inverse Fourier transform (6) can now be evaluated by distinguishing two types of singularities in the lower half ω-plane bounded by L. One may first note that the functions Φ_+ and Φ_- have in general a logarithmic singularity at the critical point where $U(y) = c$. For a given value of k, y or y_0 this corresponds to a logarithmic branch point at $\bar{\omega}(k, y) = kU(y)$, the branch cut being chosen to lie below L as sketched in figure 2(*a*). The other singularities are poles arising from the zeros of $D(\omega, k; y_0)$, i.e. the temporal eigenvalues, since k is real on F. In the case of a free shear layer with one inflection point there is, for k real, one unstable eigenvalue $\omega_1(k)$ and one stable eigenvalue $\omega_2(k)$. In the purely inviscid case the two branches $\omega_1(k)$ and $\omega_2(k)$ are complex conjugate (Drazin & Howard 1966). This symmetry no longer holds if $\omega_1(k)$ and $\omega_2(k)$ are considered to be the limit of their viscous counterparts for infinite Reynolds number (Tatsumi, Gotoh & Ayukawa 1964). We shall consider only the latter situation and assume that our solution must satisfy the equivalent Orr–Sommerfeld problem in the limit of infinite Reynolds number.

At a given wavenumber k the inverse Fourier transform (6) is the sum of two distinct terms: the continuous-spectrum contribution arises from the integral

$$\hat{G}_{\text{continuous}}(k, y, t; y_0) = \frac{1}{2\pi} \int_\Gamma \hat{\hat{G}}(k, y, \omega; y_0)\, \mathrm{e}^{-\mathrm{i}\omega t}\, \mathrm{d}\omega \tag{9}$$

along the branch cut Γ issuing from $\bar{\omega}(k)$. The discrete-spectrum contribution, which is composed of the sum of the residues evaluated at the zeros of $D(\omega, k)$, takes the form

$$\hat{G}_{\text{discrete}}(k, y, t; y_0) = \frac{2H(k)}{k} \left\{ \frac{\phi_1(y_0; k)\, \phi_1(y; k)\, \mathrm{e}^{-\mathrm{i}\omega_1(k)\, t}}{[U(y_0) - \omega_1(k)/k]\, \partial D[\omega_1(k), k]/\partial\omega} + \frac{\phi_2(y_0; k)\, \phi_2(y; k)\, \mathrm{e}^{-\mathrm{i}\omega_2(k)\, t}}{[U(y_0) - \omega_2(k)/k]\, \partial D[\omega_2(k), k]/\partial\omega} \right\}, \tag{10}$$

where $\phi_j(y; k)$ is the eigenfunction associated with the temporal eigenvalue $\omega_j(k)$. Brown & Stewartson (1980) have shown that, in a stratified flow of constant shear, the continuous spectrum decays, in the limit of zero Richardson number, as $O(t^{-2})$ for $t \to \infty$. By contrast, the discrete-mode part (10) of the solution grows exponentially with time at the temporal amplification rate $\omega_{1i}(k)$, provided that k is in the unstable range of wavenumbers. For our purposes, we shall neglect the continuous spectrum and the exponentially decaying solution in (10). The leading behaviour of the impulse response is then obtained by applying the inverse Fourier transform (5) to the first term in (10) so as to read

$$G(x, y, t; y_0) \sim \frac{1}{\pi} \int_F \frac{\phi_1(y_0; k)\, \phi_1(y; k)}{kU(y_0) - \omega_1(k)} \frac{\mathrm{e}^{\mathrm{i}[kx - \omega_1(k)\, t]}}{\partial D[\omega_1(k), k]/\partial\omega} \mathrm{d}k. \tag{11}$$

The method of steepest descent can now be applied to (11) in a manner similar to that described by Gaster (1968). The original path of integration F is deformed into two steepest-descent paths emanating respectively from the integral boundary point

$k = 0$ and the saddlepoint (k^*, ω^*), given by

$$\frac{\mathrm{d}\omega_1}{\mathrm{d}k}(k^*) = \frac{x}{t}. \tag{12}$$

As $t \to \infty$, the impulse response reduces to

$$G(x, y, t; y_0) \sim \left(\frac{2}{\pi}\right)^{\frac{1}{2}} \frac{\mathrm{e}^{\frac{1}{4}i\pi}\, \phi_1(y_0; k^*)\, \phi_1(y; k^*)\, \mathrm{e}^{i[k^* x - \omega_1(k^*)\, t]}}{[k^* U(y_0) - \omega_1(k^*)] \dfrac{\partial D}{\partial \omega}[\omega_1(k^*), k^*] \left[\dfrac{\mathrm{d}^2\omega_1}{\mathrm{d}k^2}(k^*)\, t\right]^{\frac{1}{2}}}$$
$$+ \frac{\mathrm{i}}{\pi} \frac{\phi_1(y_0; 0)\, \phi_1(y; 0)\, \mathrm{e}^{-i\omega_1(0)\, t}}{[U(y_0) - c(0)] \dfrac{\partial D}{\partial c}[c(0), 0]\, [x - c(0)\, t]}. \tag{13}$$

The leading-order contribution arising from k^* and $k = 0$ have been evaluated according to the general formulas given in Bender & Orszag (1978). The Green function takes the form of a wavepacket in the (x, t)-plane. Inside the packet the saddlepoint contribution is exponentially large and dominates the algebraically decaying $k = 0$ term in (13). Thus, among all the wavenumbers contained in the impulsive source, the flow selects, along each ray $x/t = \text{const.}$, one particular complex wavenumber k^* given by (12). The group velocity is then real and equal to x/t, and the temporal amplification rate of the wavenumber k^* along the ray reduces to $\sigma = \omega_{1i}(k^*) - k_i^* (\mathrm{d}\omega_1/\mathrm{d}k)(k^*)$. In the (x, t)-plane of figure 1, the wave packet is confined within a wedge bounded by the two rays of zero-amplification rate. Outside this wedge disturbances are algebraically decaying as given by the second term in (13). In the wedge they grow exponentially.

The nature of the instability may now be determined from figures 1 (*a*) and (*b*) by simple qualitative reasoning. In an absolutely unstable flow (figure 1 *a*) the edges of the packet travel in opposite directions, while the wavenumbers in its interior amplify exponentially. The ray $x/t = 0$ (the vertical axis in figure 1) must therefore be within the unstable wave packet. The associated complex wavenumber k_0, which by definition (12) has zero group velocity $(\mathrm{d}\omega_1/\mathrm{d}k)(k_0) = 0$, must satisfy $\omega_{1i}(k_0) > 0$. Conversely, in a convectively unstable flow, the edges of the packet travel in the same direction, e.g. in the positive-x direction as shown in figure 1 (*b*). The ray $x/t = 0$ must now lie outside the wedge and the wavenumber k_0 should satisfy $\omega_{1i}(k_0) < 0$. However, if $(\mathrm{d}\omega_1/\mathrm{d}k)(k_0) = 0$, the frequency $\omega_0 \equiv \omega_1(k_0)$ is, in general, an algebraic branch point of order two. Thus we arrive at the criterion put forward by Bers (1975): for an unstable flow to be convectively unstable, the branch-point singularities of its dispersion relation must lie in the lower half of the ω-plane. Otherwise, the system is absolutely unstable.

3. The signalling problem

To determine in which physical situations spatially growing waves are relevant, it is appropriate to consider the response of a parallel flow to a sinusoidal input of frequency ω_f, at $x = 0$, $y = y_0$, and switched on at $t = 0$. The same problem has been investigated by Gaster (1965) for the forced Orr–Sommerfeld equation. Techniques similar to those described below have also been used by Tam (1978) to study the receptivity of shear layers to sound waves.

The perturbation stream function $\psi(x, y, t; y_0)$ is now given by

$$\mathscr{L}[\psi] = \delta(x)\, \delta(y - y_0) \cos(\omega_f t)\, H(t). \tag{14}$$

As in §2, we consider instead the complex stream function

$$\Psi(x, y, t; y_0) = \left(1+\frac{\mathrm{i}}{\pi x}*\right)\psi,$$

which satisfies

$$\mathscr{L}[\Psi] = \left[\delta(x)+\frac{\mathrm{i}}{\pi x}\right]\delta(y-y_0)\cos(\omega_f t)\,H(t), \tag{15}$$

with the real response ψ being related to Ψ by the formula $\psi = \mathrm{Re}\,\Psi$. Upon application of two successive Fourier transforms (5) and (6), (15) becomes

$$\mathrm{L}[\hat{\hat{\Psi}}] = \frac{H(k)}{kU(y_0)-\omega}\left[\frac{1}{\omega-\omega_f}+\frac{1}{\omega+\omega_f}\right]\delta(y-y_0). \tag{16}$$

From (8), one immediately infers that the solution of (16) is

$$\hat{\hat{\Psi}}(k, y, \omega; y_0) = \tfrac{1}{2}\mathrm{i}\left[\frac{1}{\omega-\omega_f}+\frac{1}{\omega+\omega_f}\right]\hat{\hat{G}}(k, y, \omega; y_0). \tag{17}$$

The evaluation of $\hat{\Psi}(k, y, t; y_0)$ by contour integration in the ω-plane leads us to distinguish different elements in the response. The transient part is composed of the discrete and continuous spectra associated with the singularities of $\hat{\hat{G}}$ (see §2). The 'steady-state' response arises from the additional poles at $\omega = \pm\omega_f$. If the flow is absolutely unstable, the transient contribution will progressively overwhelm the 'steady-state' response at all points in the flow, thereby making the signalling problem physically meaningless. However, if the flow is only convectively unstable, transients will gradually move away from the source leaving a genuine observable steady-state signal. In this section we shall, henceforth, assume the instability to be convective and ignore the transient portion of the response. The residues of (17) arising from the poles at $\omega = \pm\omega_f$ yield

$$\Psi(k, y, t; y_0) \sim \tfrac{1}{2}[\hat{\hat{G}}(k, y, \omega_f; y_0)\,\mathrm{e}^{-\mathrm{i}\omega_f t}+\hat{\hat{G}}(k, y, -\omega_f; y_0)\,\mathrm{e}^{\mathrm{i}\omega_f t}]. \tag{18}$$

The inverse Fourier transform (5) can now be performed by contour integration in the k-plane. The poles of (18) are readily identified as the zeroes of $D(\pm\omega_f, k)$, i.e. the spatial eigenvalues $k(\pm\omega_f)$. To avoid some possibly confusing general notation we restrict the following discussion to the class of mixing-layer-velocity profiles considered in the next section. For these profiles there are three branches of spatial eigenvalues, $k_1^+(\omega)$, $k_1^-(\omega)$ and $k_2^+(\omega)$, which are representative of the types of eigenvalues found in more complex flows. The first two roots, $k_1^+(\omega)$ and $k_1^-(\omega)$, correspond in the ω-plane to the two Riemann sheets of the square-root singularity of the amplified branch $\omega_1(k)$. The last root $k_2^+(\omega)$ is the inverse of the stable branch $\omega_2(k)$ studied by Tatsumi *et al.* (1964). Some care needs to be exercised to determine which branches contribute on each side of the forcing location at $x = 0$. Recall that the paths of integration were initially chosen according to the sketches in figures 2(*a*) and (*b*). As pointed out by Bers (1975), the initial contour L in the ω-plane can always be placed high enough so that, when ω is on L, some of the branches (in our case $k_1^+(\omega)$ and $k_2^+(\omega)$) are in the upper-right quarter-plane and the third branch $k_1^-(\omega)$ is in the lower-right quarter-plane. As L is gradually displaced downward to coincide with the real-ω axis, the curves $k_1^+(\omega)$ and $k_1^-(\omega)$ move towards each other in the k-plane. In fact, when ω becomes real, part of the branch $k_1^+(\omega)$ necessarily lies below the real-k axis so as to give a band of spatially unstable frequencies (figures 3*a* and *b*). The loci of the spatial roots in this figure 3 are taken from the example to be discussed in the

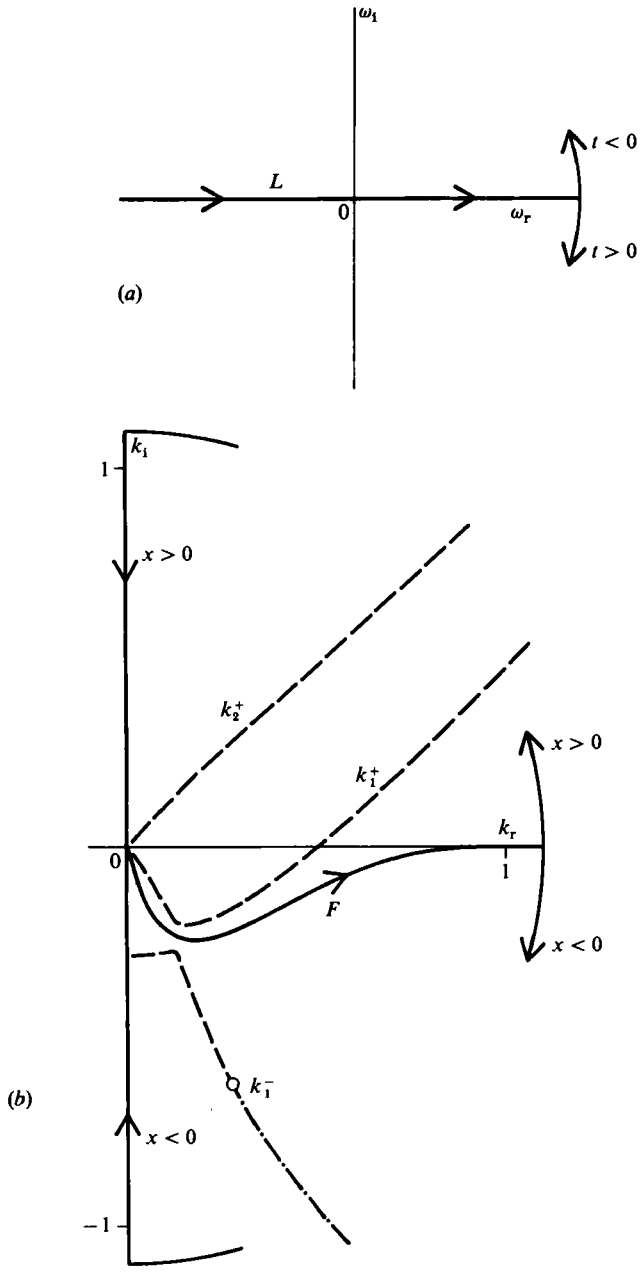

FIGURE 3. Paths of integration of the inverse Fourier transforms (5) and (6) after deformation of L onto the ω_r-axis: (*a*) complex-frequency plane; (*b*) complex-wavenumber plane. ———, loci of $k_j^+(\omega)$ and $k_1^-(\omega)$ for $\omega > 0$ (from the example of figures 7 and 8 with $R = 1.3$); —·—·—, locus of $k_1^-(\omega)$ for $\omega < 0$.

next section. In this process one must correspondingly deform the original path of integration F of figure 2(*b*) so as to stay below $k_j^+(\omega)$, $j = 1, 2$. The calculation of the inverse Fourier transform of (18) along F then proceeds in a straightforward manner. When $x > 0$, the path of integration F is deformed into a steepest-descent path, $k_r = 0$, $k_i > 0$, issuing from the integration boundary $k = 0$ (see figure 3*b*). In the limit

$x \to +\infty$ there will be two leading-order contributions: an algebraically decaying term arising from the integration boundary $k = 0$ and exponentially growing and decaying modes associated with the residues of the poles $k_j^+(\omega_f)$, $j = 1, 2$. In the limit $x \to -\infty$, the path F is deformed into the steepest-descent contour, $k_r = 0$, $k_i < 0$, issuing from $k = 0$ and similar considerations hold. The final result for $|x| \to \infty$ is:

$$\Psi(x, y, t; y_0) \sim \frac{\mathrm{i}}{2\pi x} \mathrm{Re}\{\hat{\hat{G}}(0, y, \omega_f; y_0)\, \mathrm{e}^{-\mathrm{i}\omega_f t}\}$$

$$- \sum_{j=1}^{2} \frac{\phi_j^+(y_0; \omega_f)\, \phi_j^+(y; \omega_f)\, \mathrm{e}^{\mathrm{i}[k_j^+(\omega_f)\, x - \omega_f t]}}{[k_j^+(\omega_f)\, U(y_0) - \omega_f] \dfrac{\partial D}{\partial k}[\omega_f, k_j^+(\omega_f)]} H(x)$$

$$+ \left\{ \frac{\phi_1^-(y_0; \omega_f)\, \phi_1^-(y; \omega_f)\, \mathrm{e}^{\mathrm{i}[k_1^-(\omega_f)\, x - \omega_f t]}}{[k_1^-(\omega_f)\, U(y_0) - \omega_f] \dfrac{\partial D}{\partial k}[\omega_f, k_1^-(\omega_f)]} \right.$$

$$\left. + \frac{\phi_1^-(y_0; -\omega_f)\, \phi_1^-(y; -\omega_f)\, \mathrm{e}^{\mathrm{i}[k_1^-(-\omega_f)\, x + \omega_f t]}}{[k_1^-(-\omega_f)\, U(y_0) + \omega_f] \dfrac{\partial D}{\partial k}[-\omega_f, k_1^-(-\omega_f)]} \right\} H(-x). \tag{19}$$

The spatial eigenfunctions are denoted by ϕ_j^+, $j = 1, 2$, and ϕ_1^- respectively. Since the real response ψ is obtained from Ψ by taking the real part of (19), the purely imaginary algebraic term due to $k = 0$ has no physical significance. The above reasoning presents the advantage of uniquely determining which spatial branches are pertinent to the domains $x > 0$ and $x < 0$. We conclude, as expected intuitively, that in a convectively unstable medium spatially growing waves are generated by steady periodic forcing in the range of unstable frequencies.

4. Application to a family of mixing layers

In order to illustrate the procedure, the criterion of §2 has been applied to parallel free shear layers described by the one-parameter family of velocity profiles $U(y; R) = 1 + R \tanh \frac{1}{2}y$. The cross-stream coordinate y and the velocity U are non-dimensional variables which have been scaled with respect to the momentum thickness and the average velocity between the two streams respectively. The parameter R is defined here as the ratio of the difference and the sum of the velocities of the two co-flowing streams U_1 and U_2: it is a measure of the magnitude of the shear. If $0 < R < 1$ both streams run in the same direction, while for $R > 1$ they flow in opposite directions. In the limiting case where $R = 0$ there is no shear, and, when $R = 1$, only one stream is present.

Different complex pairs (ω, k) satisfying the dispersion relation $D(\omega, k; R) = 0$, were determined by numerical integration of the Rayleigh equation, $\mathrm{L}(\phi] = 0$, together with exponentially decaying boundary conditions at $y = \pm\infty$ [see Monkewitz & Huerre 1982 for details]. At each value of R, the point of zero group velocity, $\omega_0 = \omega_1(k_0; R)$ satisfying $(\partial\omega_1/\partial k)(k_0; R) = 0$, was located by searching for the zero of the function $[k_1^+(\omega) - k_1^-(\omega)]^2$ in the complex-ω plane. It was checked that ω_0 is a square-root singularity by verifying that $|k_1^+(\omega) - k_1^-(\omega)|^2$ is locally a linear function of the distance from the branch point. As the velocity ratio R is varied, the point ω_0 describes a curve in the complex-ω plane as shown in figure 4. The associated parametric dependence of the real and imaginary parts ω_{0r} and ω_{0i} on R is displayed in figure 5. The variations of the real and imaginary parts of the wavenumber, k_{0r}

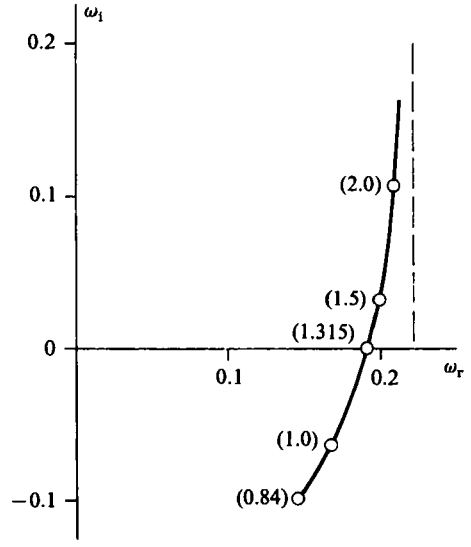

FIGURE 4. Locus of the branch point ω_0 in the complex-ω plane as a function of the velocity ratio R (in brackets). ———, large-R approximation (21).

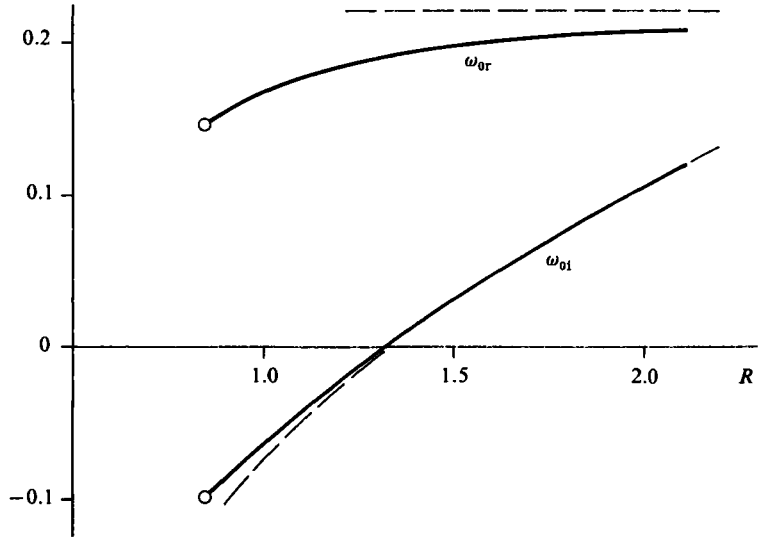

FIGURE 5. Variations of ω_{0r} and ω_{0i} with velocity ratio R. ———, large-R approximation (21).

and k_{0i}, are presented in figure 6. The curve of figure 4 crosses the real-ω axis at $\omega_r = 0.192$, which corresponds to the velocity ratio $R_t = 1.315$. When $R < R_t$, the point ω_0 lies in the lower half ω-plane and we conclude that the mixing layer $U(y; R)$ is convectively unstable. When $R > R_t$, ω_0 is in the upper half ω-plane and the mixing layer is absolutely unstable. Note that when $R < 0.84$ the branch point moves into the $k_r < 0$ half-plane, a region which is of no interest for the evaluation of physical quantities.

Large-R asymptotics of the functions $\omega_0(R)$ and $k_0(R)$ can easily be derived if one

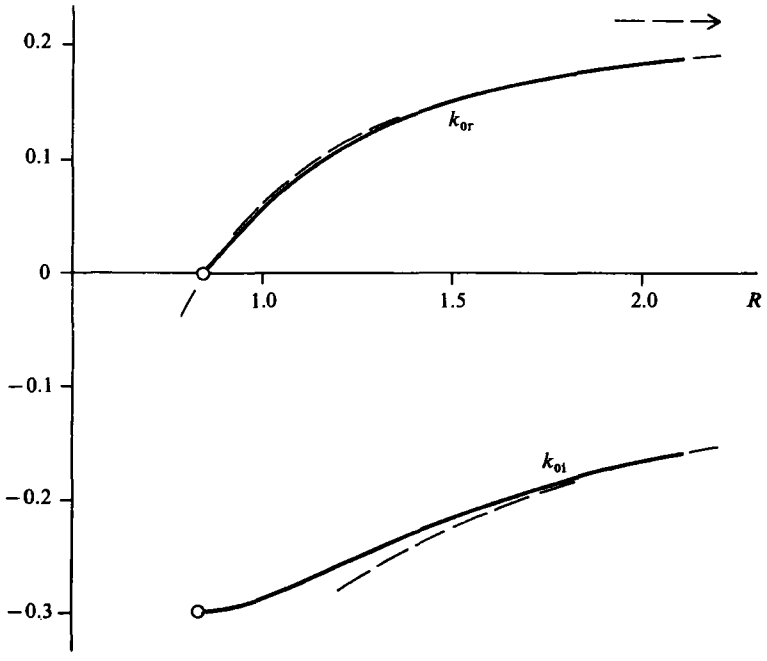

FIGURE 6. Variation of k_{0r} and k_{0i} with velocity ratio R. ———, large-R approximation (22).

notes that the dispersion relation is of the form

$$\omega = k + R\Omega(k), \tag{20}$$

where $\Omega(k)$ is the dispersion relation pertaining to $U(y) = \tanh(\frac{1}{2}y)$. It is found that, as $R \to \infty$,

$$\omega_0 \sim \mathrm{i}R\Omega_{\mathrm{i}}^{\max} + k^{\max} + \frac{\mathrm{i}}{2R}\left[\frac{\mathrm{d}^2\Omega_{\mathrm{i}}}{\mathrm{d}k^2}(k^{\max})\right]^{-1} + O(R^{-2}), \tag{21}$$

and

$$k_0 \sim k^{\max} + \frac{\mathrm{i}}{R}\left[\frac{\mathrm{d}^2\Omega_{\mathrm{i}}}{\mathrm{d}k^2}(k^{\max})\right]^{-1} + \frac{1}{2R^2}\left[\frac{\mathrm{d}^3\Omega_{\mathrm{i}}}{\mathrm{d}k^3}(k^{\max})\right]\left[\frac{\mathrm{d}^2\Omega_{\mathrm{i}}}{\mathrm{d}k^2}(k^{\max})\right]^{-3} + O(R^{-3}). \tag{22}$$

In the above formulae, $k^{\max} = 0.2225$ is the real wavenumber of maximum temporal-amplification rate, $\Omega_{\mathrm{i}}^{\max} \equiv \Omega_{\mathrm{i}}(k^{\max}) = 0.09486$, as obtained from a temporal-stability analysis [Michalke 1964) of the profile $U(y) = \tanh(\frac{1}{2}y)$. Thus, to leading order, the characteristics of the branch point coincide with those of the most-amplified temporally growing wave. The large-R approximation is compared with the numerical results in figures 5 and 6.

The configuration of the spatial branches k_1^+ and k_1^- exhibits delicate changes with velocity ratio R, which directly affect the character of the response to a periodic excitation as given in (19). When $R > 0.84$, a square-root singularity with $k_{0r} > 0$ is present in the complex-ω plane. According to the discussion of §3, there exist two spatial branches $k_1^+(\omega)$ and $k_1^-(\omega)$ which are the inverse of the temporal solution $\omega_1(k)$. However, when $0.84 < R < 1$, it is found that, for real values of ω, the branch $k_1^-(\omega)$ lies entirely in the left half-plane $k_{1r}^- < 0$. Thus, in this range of values of R, the pole

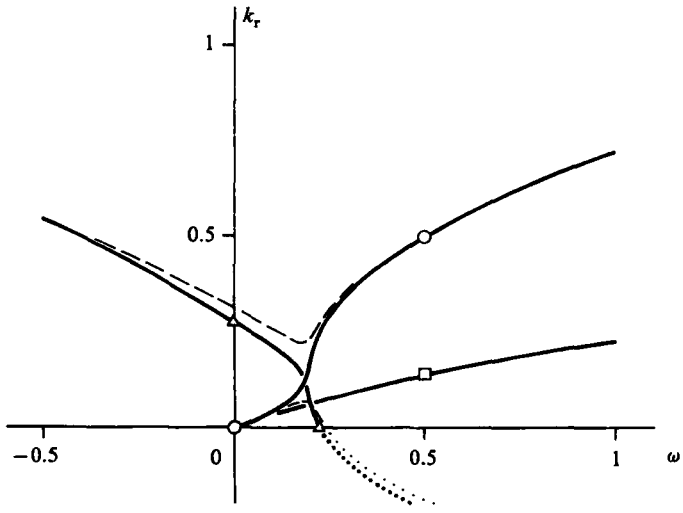

FIGURE 7. Real part of the branches k_j^+ and k_1^- *vs.* real ω for $R = 1.3$: ○——○, k_1^+; △——△, k_1^-; □——□, k_2^+; ———, branch interchange for $R = 1.4$; ....., analytic continuation into $k_r < 0$ (corresponding to solutions which become exponentially large as $|y| \to \infty$).

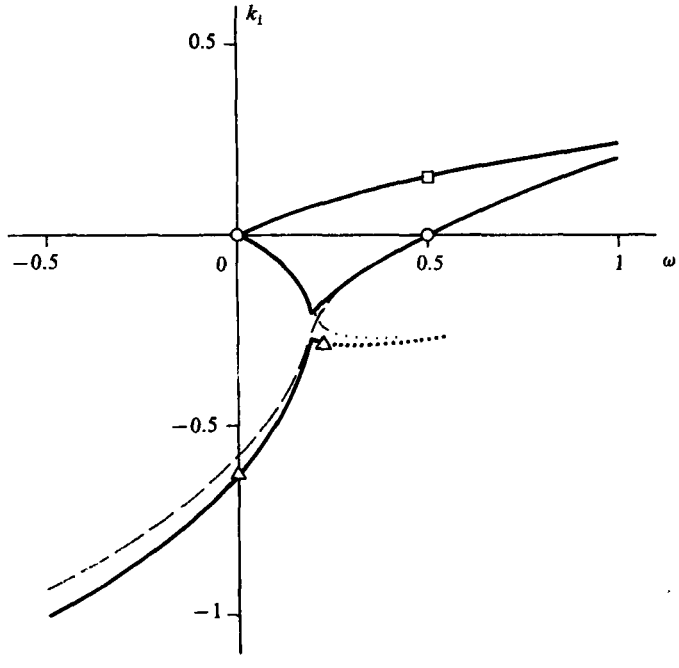

FIGURE 8. Imaginary part of the branches k_j^+ and k_1^- *vs.* real ω for $R = 1.3$. For symbols see figure 7.

k_1^- does not give rise to a residue in the evaluation of (19) and no disturbances are felt upstream of the source. But as soon as there is some counterflow, i.e. when $R > 1$, there exists a range of real frequencies, $-\infty < \omega < \omega_u$, such that $k_{1r}^-(\omega) > 0$. The upper boundary ω_u of this interval is hereby defined by $k_{1r}^-(\omega_u) = 0$. We conclude that the mode k_1^- is present upstream of the source only when $R > 1$. Numerical

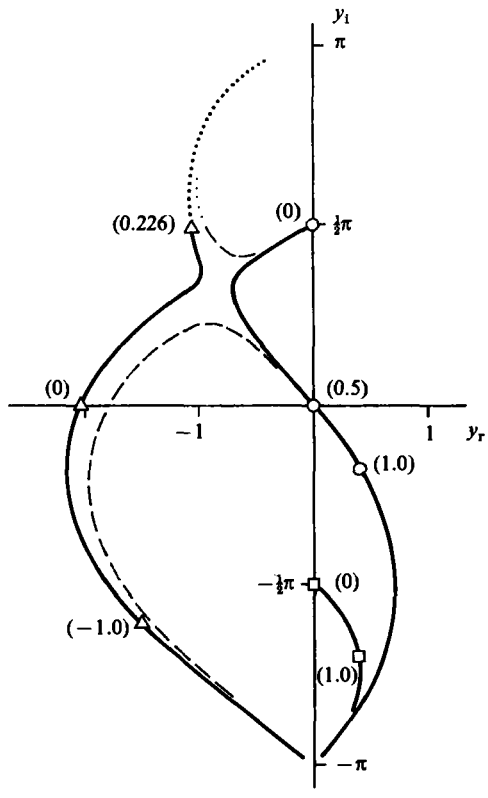

FIGURE 9. Locus of the critical points y_{cj}^{+} and y_{c1}^{-} in the complex-y plane with ω as parameter (in brackets). The symbols correspond to those of figures 7 and 8.

experiments indicate that, as $R \downarrow 1$, ω_u is negative and, to leading order, proportional to $\ln(R-1)$. For $R > 1.02$, ω_u becomes positive.

As an example, the variations with real frequency of all three eigenvalues k_1^+, k_1^- and k_2^+ have been plotted on figures 7 and 8 at $R = 1.3$, a value slightly less than $R_t = 1.315$. The trajectories of the corresponding critical points y_{c1}^+, y_{c1}^- and y_{c2}^+ in the complex-y plane are shown on figure 9. The first downstream branch k_1^+ is unstable for frequencies between 0 and 0.5 with a maximum spatial amplification rate of -0.208, almost twice the value at $R = 1$. The computation has been extended into the damped region $\omega > 0.5$ by deforming the integration path in the complex-y plane below the critical point y_{c1}^+. This procedure is the spatial analogue of the approach used by Tatsumi *et al.* (1964) in the temporal case. It amounts to considering a fully viscous critical layer in the limit of infinite Reynolds number. In the same fashion, the second downstream branch k_2^+ is obtained by integrating below y_{c2}^+ in the complex-y plane: it leads to damped disturbances downstream of the source at all excitation frequencies. Finally, the upstream branch k_1^- is seen to have a positive real part and a negative imaginary part over the entire range $\omega < \omega_u(R = 1.3) = 0.226$. Thus the amplitude of this upstream mode always decays exponentially away from the source. It is interesting to note that this branch contains modes with real phase velocities ω/k_{1r}^- of both signs. When $\omega > 0$ the wave propagates in the downstream direction towards the source. It is therefore 'amplified' in the direction of propagation and the associated critical point y_{c1}^- lies in the upper half-plane (see figure 9). When $\omega < 0$

the wave is moving in the upstream direction. Thus it is 'damped' in the direction of propagation and the critical point y_{c1}^- is in the lower half-plane. The results in this situation are again obtained by integrating below the critical point y_{c1}^-, i.e. by introducing a fully viscous critical layer. That this is possible has been verified by a local Stokes line analysis valid for small negative ω. At $\omega = 0$, the critical point lies on the real axis at $y_{c1}^- = \ln[(R-1)/(R+1)]$. This is a somewhat unusual example of a singular neutral mode with complex wavenumber: it is singular since the critical point y_{c1}^- does not coincide with the inflection point of the basic velocity profile and the eigenfunction has a logarithmic singularity at y_{c1}^-. It is also neutral since c is real (in fact equal to zero).

To conclude this section it is noted that, as soon as the velocity ratio is raised above R_t, making the flow absolutely unstable, the two branches k_1^+ and k_1^- exchange their identity across the value $\omega_{0r}(R)$ of the real frequency. This is illustrated in figures 7–9, where results at $R = 1.4$ are represented by dashed lines. When R increases above R_t, the branch point ω_0 moves into the upper half-plane and the value $\omega_{0r}(R)$ is precisely the intersection point of the real-ω axis with the branch cut emanating from ω_0.

5. Further applications and concluding remarks

From physical intuition, one might have expected the relevance of spatial theory to be restricted to shear generated by streams moving in the same direction ($0 < R < 1$). According to the results of the previous section, spatially growing waves are likely to be observed in the presence of a small counterflow, as long as its magnitude $|U_2|$ is such that $|U_2/U_1| < 0.136$. For any larger counterflow, the mixing layer is absolutely unstable and should be described in terms of temporally growing disturbances.

In most experimental studies on transitional shear layers (Browand 1966; Freymuth 1966; Miksad 1972; Ho & Huang 1982), the basic flow is generated by the mixing of two streams of different velocity downstream of a splitter plate. In this case $0 < R < 1$ and spatial theory does compare very favourably with experimental observations. The case $R > 1$ could be realized by applying suction on the back face of a backward-facing step, an experiment which has, to our knowledge, not yet been tried. It is interesting to note that temporally evolving mixing layers can be obtained experimentally by tilting a tank filled with a stably stratified fluid (Thorpe 1971). In such a case, the initial Richardson number can be made small enough to warrant qualitative comparison with the unstratified analysis. These flows are such that $R \gg 1.315$ and are therefore absolutely unstable. The growth rates observed by Thorpe (1971) are found to be 25% lower than those predicted by temporal theory but the measured wavenumber is very close to the value for the most-amplified wave in a tanh shear layer.

Other flows similarly defy physical intuition when one wishes to establish whether they are absolutely or convectively unstable. However, an answer to this question is essential to determine if a low-level control input, such as forcing applied at the trailing edge in a mixing layer with $R < R_t$, can effectively influence the global development of the flow. We shall briefly discuss two other examples: wake flows and hot jets.

Betchov & Criminale (1966) and Mattingly & Criminale (1972) have previously analysed the branch point ω_0 arising in the family of wake profiles $U(y; Q) = 1 - Q\,\mathrm{sech}^2 y$. From their results it can be inferred that the wake becomes absolutely unstable when $Q \geqslant 0.94$, i.e. below the value $Q = 1$ giving rise to a

counterflow in the centre of the wake. In other words, wake profiles in the range $0.94 < Q < 1$, which represent unidirectional flows with a positive velocity everywhere, are nonetheless absolutely unstable! It was also noted in these investigations that at the branch point (ω_0, k_0) the Wronskian D in (8) has a *double* zero. Thus, at (ω_0, k_0), a non-trivial solution $\hat{G}$ can be obtained for zero pulse strengths, which indicates a resonance phenomenon analogous to acoustic organ-pipe resonance. The authors then conclude that the wake response should be primarily determined by this resonance, giving rise in general to an amplified ($\omega_{0i} > 0$) or decaying ($\omega_{0i} < 0$) wave at a *complex* frequency ω_0. In a recent development of these ideas, Koch (1983, 1985) has convincingly shown, by comparison with experiments in the wake of a blunt trailing edge, that the response is dominated by a resonance at a *real* frequency ω_0. In Koch's analysis, a quasi-parallel assumption is made in the measured-mean-velocity profiles to demonstrate that, owing to a gradual fill-up of the wake, the flow actually contains both absolutely and convectively unstable regions. The real resonance frequency is predicted by calculating the branch point (ω_0, k_0) at the downstream station x_0 where the flow makes a transition from absolute to convective instability. It should be recalled that at the branch point the group velocity is zero and some of the disturbance energy coming from upstream can be reflected at x_0 as part of a feedback loop between the body and x_0 (see e.g. the discussion in appendix B of Lighthill 1981). Thus it can be inferred that the *local* resonance at x_0 is an essential link in a *global* resonance or self-sustained feedback loop. Finally, to strengthen a point made earlier, it is worth mentioning that the dominant frequency in bluff-body wakes is relatively independent of the particular facility, i.e. its background turbulence intensity and spectral content.

In striking contrast to this relative insensitivity of wakes is the facility dependence of most free jets. Cold jets with $R < 1$ are convectively unstable and thus very sensitive to low-level forcing, as extensively documented in the literature. We wish to show how this situation can change dramatically when the jet is heated. Only a brief outline is given here with a more complete report by one of us (PAM) to follow later. The stability of a hot plug-flow jet bounded by a cylindrical vortex sheet has already been investigated by Michalke (1970) as a function of Mach number M and temperature ratio T^*. The parameter T^* is defined as the ratio between ambient and jet static temperatures ($T^* < 1$ for a hot jet) and S_D will denote the Strouhal number based on angular frequency ω, jet velocity U_j and jet diameter D. The discussion is restricted to axisymmetric modes at $M = 0$. As shown on figure 10, adapted from Michalke's figures 2 and 3, two modes exchange their identity across the value $S_D \approx 3$, when the temperature ratio T^* decreases from 0.7 to 0.6. This behaviour is very similar to the interchange displayed in figures 7 and 8 for the family of mixing layers. It led us to believe that the jet becomes absolutely unstable if sufficiently hot. Indeed, it was confirmed numerically that, in analogy with the case of mixing layers, a square-root branch point crosses the real-S_D axis at $S_{D,0} = 3.052$ as the temperature ratio T^* decreases through the transition value $T_t^* = 0.658$. As T^* decreases from 0.7 to 0.6, the branch point moves into the upper-half S_D-plane. Stability calculations conducted for a finite shear-layer-momentum thickness Θ by Michalke (1971) suggest that the transition temperature ratio T_t^* is relatively independent of Θ as long as $\Theta/D \ll 1$ (see Michalke's figure 12). It is also noted in passing that, even for the cold jet, the (time-damped) branch point still has an effect by causing low-frequency disturbances to travel faster than the jet (see figure 6 of Bechert & Pfitzenmaier 1975). The arguments presented here may have implications for the control of noise in jets. For instance, only a strong tempering of the flow, such as

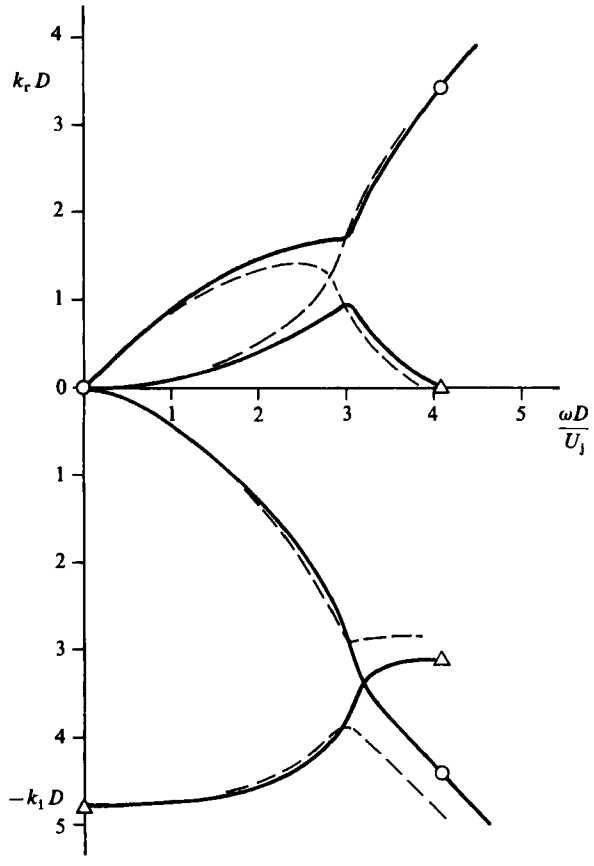

FIGURE 10. The wavenumbers k_1^+ and k_1^- for axisymmetric disturbances on a compressible cylindrical vortex sheet (adapted from Michalke 1970) with $M = 0$ and $T^* = 0.7$; O——O, k_1^+; △——△, k_1^-; ———, branch interchange for $T^* = 0.6$.

a daisy-type nozzle, is likely to alter the noise radiation characteristics of an absolutely unstable hot jet with $T^* < T_t^*$. This type of nozzle does produce a cooler jet which, for $T^* > T_t^*$, loses its region of absolute instability, thereby providing a possible explanation for the success of such a device. Finally, we speculate that the velocity ratio will also strongly influence the characteristics of hot jets. Situations are conceivable where an absolutely unstable hot jet on a test stand ($R = 1$) could become convectively unstable in flight ($R < 1$), thus complicating further the problem of flight effects on jet mixing noise.

Further applications of the reasoning outlined in this study are numerous. For instance, it is not entirely clear whether the presence of Görtler vortices along concave walls is the result of a temporal instability or of the spatial response to a periodic forcing. The approach presented here might be able to settle the issue. Finally, we note that the generalization of these concepts to nonlinear instability phenomena is an open question (see Weissman 1979 for a discussion of weakly nonlinear Kelvin–Helmholtz instability).

P. Huerre wishes to acknowledge the financial support of the National Science Foundation under grant CME-7916162.

REFERENCES

BECHERT, D. & PFITZENMAIER, E. 1975 On wavelike perturbations in a free jet travelling faster than the mean flow in the jet. *J. Fluid Mech.* **72**, 341–352.

BENDER, C. M. & ORSZAG, S. A. 1978 *Advanced Mathematical Methods for Scientists and Engineers.* McGraw-Hill.

BERS, A. 1975 Linear waves and instabilities. In *Physique des Plasmas* (ed. C. DeWitt & J. Peyraud), pp. 117–213. New York: Gordon and Breach.

BETCHOV, R. & CRIMINALE, W. O. 1966 Spatial instability of the inviscid jet and wake. *Phys. Fluids* **9**, 359–362.

BRIGGS, R. J. 1964 Electron-stream interaction with plasmas. *Research Monograph No.* 29. Cambridge, Mass: M.I.T. Press.

BROWAND, F. K. 1966 An experimental investigation of the instability of an incompressible, separated shear layer. *J. Fluid Mech.* **26**, 281–307.

BROWN, S. N. & STEWARTSON, K. 1980 On the algebraic decay of disturbances in a stratified shear flow. *J. Fluid Mech.* **100**, 811–816.

CASE, K. M. 1960 Stability of inviscid Couette flow. *Phys. Fluids* **3**, 143–148.

CHIMONAS, G. 1979 Algebraic disturbances in stratified shear flows. *J. Fluid Mech.* **90**, 1–19.

DRAZIN, P. G. & HOWARD, L. N. 1966 Hydrodynamic stability of parallel flow of inviscid fluid. *Adv. Appl. Mech.* **9**, 1–89.

DRAZIN, P. G. & REID, W. H. 1981 *Hydrodynamic Stability.* Cambridge University Press.

FREYMUTH, P. 1966 On transition in a separated laminar boundary layer. *J. Fluid Mech.* **25**, 683–704.

GASTER, M. 1965 On the generation of spatially growing waves in a boundary layer. *J. Fluid Mech.* **22**, 433–441.

GASTER, M. 1968 Growth of disturbances in both space and time. *Phys. Fluids* **11**, 723–727.

GASTER, M. 1975 A theoretical model of a wave packet in the boundary layer on a flat plate. *Proc. R. Soc. Lond.* A **347**, 271–289.

GASTER, M. 1980 The propagation of wave packets in laminar boundary layers: asymptotic theory for non-conservative wave systems. *Preprint*, National Maritime Institute, Teddington, England.

HO, C. M. & HUANG, L. S. 1982 Subharmonics and vortex merging in mixing layers. *J. Fluid Mech.* **119**, 443–473.

KOCH, W. 1983 Organized structures in wakes and jets – An aerodynamic resonance phenomenon? *Proc. 4th Symp. on Turb. shear Flows at Karlsruhe.* Springer.

KOCH, W. 1985 Local instability characteristics and frequency determination of self-excited wake flows. *J. Sound and Vib.* **99**, in press.

LIGHTHILL, J. 1981 Energy flow in the cochlea. *J. Fluid Mech.* **106**, 149–213.

MATTINGLY, G. E. & CRIMINALE, W. O. 1972 The stability of an incompressible two-dimensional wake. *J. Fluid Mech.* **51**, 233–272.

MERKINE, L. O. 1977 Convective and absolute instability of baroclinic eddies. *Geophys. Astrophys. Fluid Dyn.* **9**, 129–157.

MICHALKE, A. 1964 On the inviscid instability of the hyperbolic tangent velocity profile. *J. Fluid Mech.* **19**, 543–556.

MICHALKE, A. 1965 On spatially growing disturbances in an inviscid shear layer. *J. Fluid Mech.* **23**, 521–544.

MICHALKE, A. 1970 A note on the spatial jet-instability of the compressible cylindrical vortex sheet. *DLR research rep.* FB-70-51.

MICHALKE, A. 1971 Instabilität eines kompressiblen runden Freistrahls unter Berücksichtigung des Einflusses der Strahlgrenzschichtdicke. *Z. Flugwiss.* **19**, 319–328.

MIKSAD, R. W. 1972 Experiments on the nonlinear stages of free shear layer transition. *J. Fluid Mech.* **56**, 695–719.

MONKEWITZ, P. A. & HUERRE, P. 1982 Influence of the velocity ratio on the spatial instability of mixing layers. *Phys. Fluids* **25**, 1137–1143.

TAM, C. K. W. 1978 Excitation of instability waves in a two-dimensional shear layer by sound. *J. Fluid Mech.* **89**, 357–371.

TATSUMI, T., GOTOH, K. & AYUKAWA, K. 1964 The stability of a free boundary layer at large Reynolds numbers. *J. Phys. Soc. Japan* **19**, 1966–1980.

THORPE, S. A. 1971 Experiments on the instability of stratified shear flows: immiscible fluids. *J. Fluid Mech.* **46**, 299–319.

WEISSMAN, M. A. 1979 Nonlinear wave packets in the Kelvin–Helmholtz instability. *Phil. Trans. R. Soc. Lond.* A **290**, 639–681.